AGU PUBLICATIONS

Geophysical Research Letters

RESEARCH LETTER
10.1002/2016GL067720

Key Points:
- Detailed observations of exceptional daily melt rates on the Greenland ice sheet in July 2012
- We show this exceptional melt was dominated by nonradiative energy fluxes
- Conventional models underestimate melt episodes dominated by nonradiative energy fluxes

Supporting Information:
- Supporting Information S1

Correspondence to:
R. S. Fausto,
rsf@geus.dk

Citation:
Fausto, R. S., D. van As, J. E. Box, W. Colgan, P. L. Langen, and R. H. Mottram (2016), The implication of nonradiative energy fluxes dominating Greenland ice sheet exceptional ablation area surface melt in 2012, *Geophys. Res. Lett.*, *43*, 2649–2658, doi:10.1002/2016GL067720.

Received 8 JAN 2016
Accepted 19 FEB 2016
Accepted article online 24 FEB 2016
Published online 16 MAR 2016

The implication of nonradiative energy fluxes dominating Greenland ice sheet exceptional ablation area surface melt in 2012

Robert S. Fausto[1], Dirk van As[1], Jason E. Box[1], William Colgan[2], Peter L. Langen[3,4], and Ruth H. Mottram[3]

[1]Geological Survey of Denmark and Greenland (GEUS), Copenhagen, Denmark, [2]Department of Earth and Space Sciences and Engineering, York University, Toronto, Ontario, Canada, [3]Danish Meteorological Institute (DMI), Copenhagen, Denmark, [4]Niels Bohr Institute, University of Copenhagen, Copenhagen, Denmark

Abstract During two exceptionally large July 2012 multiday Greenland ice sheet melt episodes, nonradiative energy fluxes (sensible, latent, rain, and subsurface collectively) dominated the ablation area surface energy budget of the southern and western ice sheet. On average the nonradiative energy fluxes contributed up to 76% of daily melt energy at nine automatic weather station sites in Greenland. Comprising 6% of the ablation period, these powerful melt episodes resulted in 12–15% of the south and west Greenland automatic weather station annual ablation totals. Analysis of high resolution (~5 km) HIRHAM5 regional climate model output indicates widespread dominance of nonradiative energy fluxes across the western ablation area during these episodes. Yet HIRHAM5 still underestimates melt by up to 56% during these episodes due to a systematic underestimation of turbulent energy fluxes typical of regional climate models. This has implications for underestimating future melt, when exceptional melt episodes are expected to occur more frequently.

1. Introduction

Understanding the Greenland ice sheet surface climate response is crucial for reducing uncertainties in future predictions of both magnitude and rate of global sea level change [*Dutton et al.*, 2015] and freshwater flux [*Lenaerts et al.*, 2015]. The rate of Greenland ice sheet mass loss has accelerated over the past decades [*Tedesco et al.*, 2013; *Khan et al.*, 2015], and in recent years, the surface components of the ice sheet's mass budget have become the dominant source of ice loss, outpacing the ice dynamic component [*Enderlin et al.*, 2014; *Andersen et al.*, 2015].

Partly due to two exceptional melt episodes in July 2012 set new records for ice sheet surface melt area and ice mass loss [*Tedesco et al.*, 2013]. Satellite observations revealed more than 98% of the ice sheet surface was melting on 12 July 2012, which was unprecedented in the 1978 present satellite record [*Nghiem et al.*, 2012]. This widespread melt in the accumulation area was enhanced by low-level liquid clouds [*Bennartz et al.*, 2013] promoted by the advection of anomalously warm and moist air over Greenland [*Neff et al.*, 2014], which decreased the firn's ability to retain meltwater [*Machguth et al.*, 2016]. Deposition of wildfire black carbon further promoted melt through enhanced sunlight absorption [*Keegan et al.*, 2014]. Projections suggest that such melt episodes will become increasingly frequent in coming decades [*Collins et al.*, 2013; *McGrath et al.*, 2013].

In situ measurements from ice sheet-automated weather station sites offer insight and accuracy into the surface mass budget (SMB) and the surface energy budget (SEB), while regional climate model (RCM) simulations provide wider spatial and temporal coverage. Yet high-horizontal resolution is necessary in SMB modeling to resolve the sharp SMB and SEB spatial gradients typical of the ice sheet ablation area.

The surface energy budget consists of nonradiative (sensible, latent, rain, and subsurface) and radiative (shortwave and longwave) energy fluxes. Distinguishing the contribution of nonradiative and radiative energy fluxes in melt over the Greenland ice sheet is important to understand ice sheet surface climate sensitivity, especially in the ablation area, where the majority of melt occurs [e.g., *Fausto et al.*, 2012a]. Under warmer and wetter climate conditions, nonradiative energy fluxes, hereafter called E_{NonRad}, throughout changes in atmospheric general circulation, may increase in importance over the ice sheet [*Van den Broeke et al.*, 2008, 2011; *Hartmann et al.*, 2013]. There is evidence that E_{NonRad} fluxes are important over sea ice surfaces

Table 1. PROMICE Station Metadata, 2012 Ablation and Contribution to Ablation During Melt Episodes E1 and E2 at PROMICE AWS Sites

Station	Latitude (°N)	Longitude (°W)	Elevation (m asl)	2012 Ablation (m ice eq.)	Episode1 (E1) (m ice eq.)	Episode2 (E2) (m ice eq.)	E1 + E2 (% of Total Ablation)
KPC_L[a]	79.911	24.084	370	3.3	-	-	-
KPC_U[b]	79.834	25.168	870	0.3	-	-	-
SCO_L[c]	72.225	26.818	470	3.6	0.1	0.1	6
SCO_U[c]	72.394	27.248	980	2.9	0.1	0.1	7
TAS_L[c]	65.641	38.898	260	4.3	0.2	0.1	7
TAS_U[a]	65.699	38.867	570	3.7	-	-	-
QAS_L	61.031	46.849	290	8.5	0.9	0.3	14
QAS_U[a]	61.177	46.818	900	2.1	-	-	-
NUK_L[a]	64.483	49.540	530	6.9	-	-	-
NUK_U	64.512	49.262	1130	3.3	0.3	0.2	15
KAN_L	67.096	49.944	680	4.7	0.4	0.2	13
KAN_M	67.067	48.828	1270	2.1	0.2	0.1	14
UPE_L	72.893	54.295	220	3.3	0.3	0.1	12
UPE_U	72.889	53.560	950	2.8	0.3	0.1	14
THU_L[a]	76.400	68.266	570	2.5	-	-	-
THU_U[a]	76.420	68.145	770	1.2	-	-	-

[a]Daily measurements are unavailable either due to power failure, damaged radiometer, or damaged ablation sensor.
[b]Daily ablation measurements are smaller than the uncertainty of 0.04 m ice eq.
[c]Radiation dominated ablation.

[*Tjernström et al.*, 2015]. Yet there may be a systematic underestimation in turbulent energy fluxes over ice surfaces in RCMs [e.g., *Lüpkes et al.*, 2012; *Elvidge et al.*, 2015; *Fettweis et al.*, 2011; *Noël et al.*, 2015].

Here we investigate atmospheric forcing of ice melt during two exceptional 2012 melt episodes as analogs for future warming. The two multiday episodes are 8–11 July (E1) and 27–28 July (E2), respectively. We compare local in situ ablation rates measured at automatic weather stations (AWSs) located in the ablation area of the Greenland ice sheet (Table 1). We draw on a HIRHAM5 regional climate model simulation to examine the spatial distribution of the 2012 exceptional melt episodes across the ice sheet in terms of SEB components. The SEB approach enables us to rank the individual energy sources contributing to melt as well as to evaluate the accuracy of melt modeled by an AWS observation-driven 1-D SEB model and by HIRHAM5 during exceptional melt episodes.

2. Methods

2.1. Observation-Driven 1-D Surface Energy Budget Model

In situ observations from the Programme for Monitoring of the Greenland Ice Sheet (PROMICE) network of AWSs [*Ahlstrøm et al.*, 2008] are used in this study (supporting information). The AWSs measure meteorological quantities needed for SMB closure, as well as accumulation and ablation [*Van As et al.*, 2012] (Table 1 and Figure S1). During the summer 2012, we had 16 PROMICE stations operating in the ablation zone of the Greenland ice sheet. Unfortunately, some of the daily measurements were unavailable either due to power failure, damaged radiometer, or damaged ablation sensor. This resulted in 12 out of 16 for SEB estimation (Table S1) and 9 out 16 for ablation measurements (Tables 1 and S2).

Using hourly-averaged AWS data, we force a SEB model, hereafter 1-D SEB_{AWS}, to quantify and rank the energy sources contributing to surface ablation at 12 PROMICE sites (Figure 1) over the 2012 ablation season [*Van As et al.*, 2012]. The energy sources considered in the 1-D SEB_{AWS} are net short and net longwave radiation, sensible heat, latent heat, rain, and subsurface energy fluxes.

Measurement errors, which vary by sensor, contribute to uncertainty in both SEB and SMB calculations. The largest stated uncertainty is the manufacturer-reported Kipp and Zonen CNR1/CNR4 radiometer (10% for daily totals) but has been independently evaluated as smaller (5% for daily totals) when used in ice sheet settings [*Van den Broeke et al.*, 2004; *Van As et al.*, 2012]. SEB model uncertainties also exist, such as those pertaining to the aerodynamic roughness length for momentum (z_0), which is used in the parameterization of the turbulent energy fluxes of latent and sensible heat. z_0 is conventionally set to constant values for either

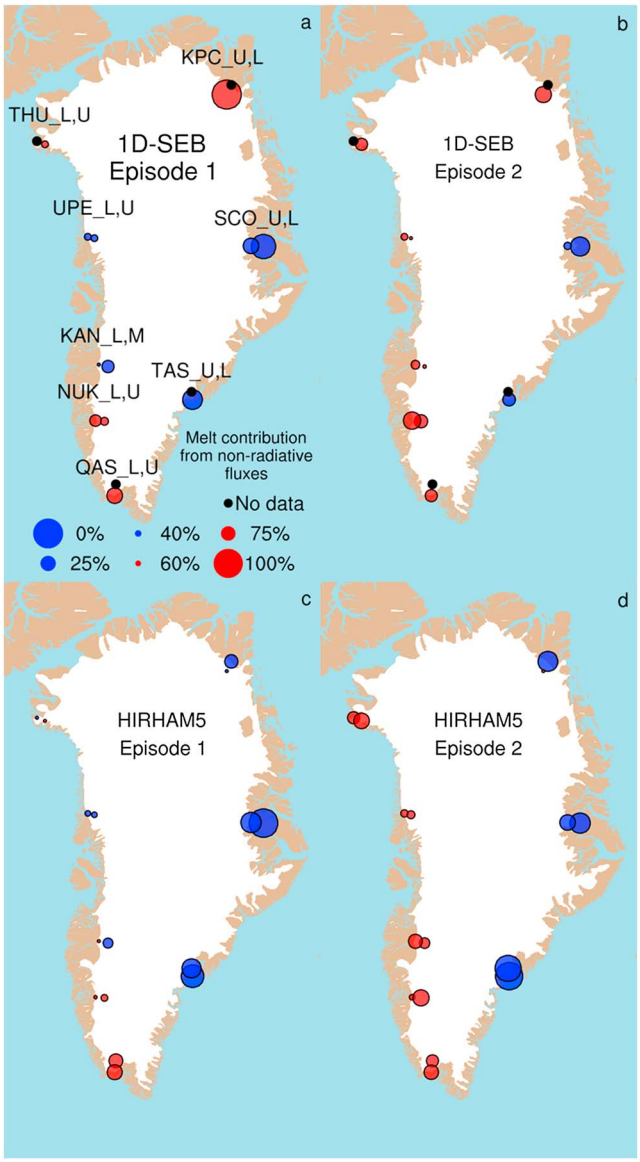

Figure 1. Relative surface energy contribution of E_{NONRAD} to available melt energy during episodes E1 and E2 for 1-D SEB_{AWS} and HIRHAM5 at PROMICE sites. Red means nonradiative fluxes dominate, blue means radiative fluxes dominate, and that the scaling of the symbol is based on the fraction of these fluxes, e.g., large symbols means 100% radiative and nonradiative fluxes, respectively. Graphics illustrate the values in Table S1.

snow or ice surfaces [*Brock et al.*, 2006], which is an oversimplification [*Smeets and Van den Broeke*, 2008; *Lüpkes et al.*, 2012]. Acknowledging this limitation, we adopt z_0 values of $5 \cdot 10^{-4}$ m for snow and $5 \cdot 10^{-3}$ m for ice at PROMICE AWS sites [*Brock et al.*, 2006], which minimizes the discrepancy between modeled and observed total ablation over the melt season. Another uncertainty in our SMB calculation is precipitation, which was not directly measured, and is therefore prescribed by HIRHAM5 (supporting information).

2.2. Regional Climate Model Surface Energy Budget

We compare HIRHAM5 SEB data to those from the PROMICE AWS using bilinear interpolation of the gridded RCM fields to the PROMICE sites, using only glacier surface-type grid cells. While a clear strength of the RCM is complete spatial coverage, its day-to-day calculation of melt at a specific site is inherently less accurate than the observation-driven 1-D SEB_{AWS} [*Lucas-Picher et al.*, 2012; *Langen et al.*, 2015] (supporting information). RCM uncertainties stem from cloud radiative effects, vertical gradients in the shallow atmospheric boundary layer, or surface albedo parameterization [e.g., *Fettweis et al.*, 2011]. We minimize RCM albedo error by incorporating daily observed Moderate Resolution Imaging Spectroradiometer (MODIS) MOD10A1 surface albedo denoised after *Box et al.* [2012] (supporting information). In HIRHAM5, z_0 is set to a constant value of 10^{-3} m for both snow and bare glacier ice, within the z_0 for snow and ice adopted in the 1-D SEB_{AWS} [*Roeckner et al.*, 2003].

The modeled SEB and SMB from the 1-D SEB_{AWS} and HIRHAM5 are evaluated by comparing the calculated melt rates to independent in situ ablation measurements.

3. Results and Discussion

3.1. In Situ Observed Melt Rates

Table 1 illustrates the regional variation of ice ablation for the 2012 melt season from the PROMICE in situ ablation observations located in the ablation area. The annual ablation values are calculated as the height difference between the end-of-melt-season surface level in the given year and the year before. The same approach is used to calculate total ablation for each of the two episodes. We require the daily ablation measurements to be larger than the uncertainty/melt detection of 0.04 m ice (equivalent) [*Fausto et al.*,

2012b], which resulted in data detectable on a daily interval from nine values for 16 weather stations. The uncertainty in ablation totals is thus 0.06 m ice eq. $\left(\sqrt{0.04^2 + 0.04^2}\right)$.

Ablation varies with elevation, but there are also considerable latitudinal differences as the Greenland ice sheet stretches from the upper midlatitudes (~60°N) to the high Arctic (~82°N). The largest total observed ice ablation in 2012 was 8.5 m ice eq. at QAS_L, which was 9% less than the 2010 value. This interannual variability may be attributed to larger winter snow accumulation in 2012, which maintained high surface albedo by delaying bare ice exposure during the melt season. The smallest 2012 ice ablation (0.3 m) was observed at KPC_U (Table 1). Annual 2012 ablation totals for the southern part of Greenland amount to 3–8 m (NUK_L, QAS_L, and TAS_L stations), while ablation totals at the more northerly SCO_L, UPE_L, THU_L, and KPC_L stations amount to 3–4 m at low altitudes (below 500 m asl). Ablation totals at the upper stations (above 500 m asl) amount to 2–4 m in the south (KAN_M, NUK_U, QAS_U, and TAS_U) and 0.3–3 m in the North (KPC_U, SCO_U, UPE_U, and THU_U) (Table 1). At all PROMICE sites, the 2012 ice ablation season started in late May to mid-July, following approximately 4 weeks of snow melt. Height measurements confirm that snow did not accumulate at the PROMICE sites during the relatively warm 2012 summer. The observed average daily melt rate over the summer melt season ranged over an order of magnitude, from 0.08 m ice eq. d^{-1} (~280 W m^{-2}, energy available for melt at QAS_L) to 0.007 m ice eq. d^{-1} (~23 W m^{-2}, energy available for melt at KPC_U). The average daily melt rate for all AWS in episodes E1 and E2 was 0.08 m and 0.07 m ice eq. d^{-1}, respectively.

At the southern and western PROMICE sites (QAS, NUK, KAN, and UPE), the melt episodes E1 and E2 were collectively responsible for 12–15% of the annual ablation totals whereas these episodes only contributed 6–7% for the eastern PROMICE sites (Table 1).

3.2. Spatial Patterns of Nonradiative Energy Dominance on Melt

Comparison of SEB components illuminates dominant physical processes in the July 2012 exceptional melt episodes. We separate the radiative and the nonradiative energy sources and estimate their relative contribution to available melt energy (E_m). Figure 1 illustrates the relative melt contribution from all available E_{NonRad} sources at PROMICE sites for the 1-D $\mathrm{SEB_{AWS}}$ and HIRHAM5 models, respectively. Common for both models is that E_m was dominated by radiative energy sources in east and southeast Greenland, while south, southwest, and northwest Greenland is dominated by E_{NonRad} (Figure 1). KPC_U has the largest mismatch in the sum of radiative and nonradiative energy fluxes between 1-D SEBAWS and HIRHAM5 (Table S1), which is due to the net energy fluxes being small yielding large relative differences.

3.2.1. 1-D $\mathrm{SEB_{AWS}}$

On the western slope of the ice sheet, the E_{NonRad} contribution to E_m decreases with latitude and elevation, ranging from a maximum of 76% at QAS_L to 29% at KAN_M (~67°N and ~1270 m asl) and 38% at UPE_U (~73°N but lower in elevation at ~960 m asl). At the eight western PROMICE stations, we estimate that E_{NonRad} contributed on average 60 ± 14% of melt energy during the two 2012 exceptional melt episodes (Table S1). Given that absorbed solar radiation is the primary energy source of melt on an annual basis, the influence of intra-annual and interannual variability in air temperature and other variables on ablation is of secondary importance [*Van den Broeke et al*., 2011]. Yet during the two melt episodes we focus on, which together resulted in ~14% of annual ice ablation (Table 1), the nonradiative (sensible, latent, rain, and subsurface) energy fluxes were the primary control of melt with a contribution of 53 ± 16% and 66 ± 8%, respectively, averaged for the eight western AWSs for episodes E1 and E2, respectively (Tables 1).

Since the 1-D $\mathrm{SEB_{AWS}}$ calculation uses observed radiative fluxes with 10% absolute error (most likely less) [*Van den Broeke et al*., 2004], it is reasonable to conclude that the $\mathrm{SEB_{AWS}}$ melt underestimation (Table S2) is due to underestimating E_{NonRad} surface heating (Table S1), especially when E_{NonRad} attains anomalous values during the exceptional episodes. We speculate that the melt underestimation during the exceptional melt episodes originates from inadequate stratification corrections to the semilogarithmic surface layer profiles of wind, temperature, and humidity from the Monin-Obukov similarity theory, which affects the calculated sensible and latent energy fluxes [*Andreas*, 2002; *Lüpkes et al*., 2012; *Elvidge et al*., 2015].

3.2.2. HIRHAM5

HIRHAM5 offers a complete spatial coverage of SEB and SMB. Figure 2a illustrates the spatial distribution of the difference between E_{NonRad} and net radiative (shortwave and longwave) fluxes of melt energy for both

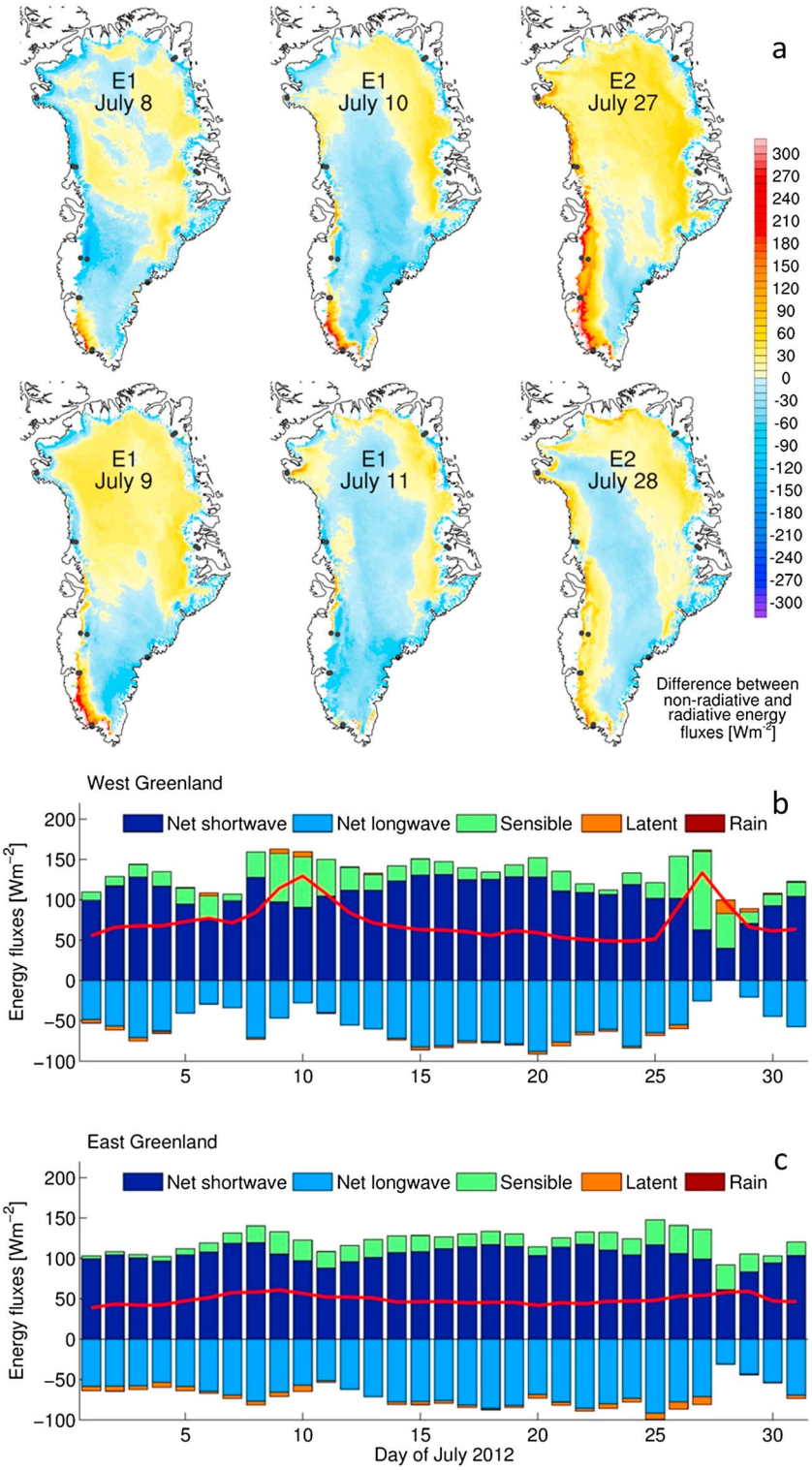

Figure 2. (a) HIRHAM5 spatial distribution of the difference between nonradiative (sensible, latent, rain, and subsurface) energy fluxes minus the radiative (net shortwave and net longwave) energy fluxes during the two melt episodes (8–11 July 2012) and (27–28 July 2012). Black dots indicate individual AWS locations. (b and c) Average daily energy flux for each component for grid points with more than 1 mm w eq. melt in HIRHAM5 for West and East Greenland, respectively. Black line is energy available for melt.

episodes (Figure 1 and Table S1). The energy flux magnitudes for HIRHAM5 are, in general, lower than the 1-D SEB_{AWS} values; however, the average absolute difference between the two modeled estimates of the nonradiative contribution to melt is ~11% (Table S1). This indicates that the variability of nonradiative fluxes in the 1-D SEB_{AWS} and HIRHAM5 model is about the same, lending confidence to the spatial pattern in Figure 2a. The RCM suggests that melt during the two episodes was dominated by E_{NonRad} over the western ablation area and radiative fluxes along the eastern margin (Figure 2a). Moreover, HIRHAM5 output also shows that the dominance of E_{NonRad} on melt decreases with elevation during these events, most notably along the southern and western ice sheet margin, in line with AWS observations.

During the two episodes, the large longitudinal contrast in nonradiative energy fluxes contribution to surface melt stem from anomalously warm and moist southern air flow being transferred onto the western ice sheet by atmospheric flow (Figure 2b) [*Neff et al*., 2014; *Bonne et al*., 2015], while east Greenland was dominated by stable weather with relatively low cloud cover and high solar radiation (Figure 2c) [*Fettweis et al*., 2013; *Tedesco et al*., 2013].

Since episode E1 consists of 4 days, the spatial illustration reflects more complex patterns than E2 as different areas of the ice sheet were dominated by nonradiative fluxes during different days (Figures 1c, 1d, and 2a). However, most of the melt was due to nonradiative fluxes in the south and southwestern part of Greenland with a latitudinal decrease, except for THU_U, of E_{NonRad} influence as the E1 progressed northward, while episode E2 affected simultaneously all of western part of the ice sheet. The average monthly difference between nonradiative and radiative fluxes for July 2012 in comparison to the July 2000–2014 average again highlights not only the dominance of nonradiative energy fluxes in the ablation area of south and west Greenland but also the dominance of radiative energy fluxes in the percolation areas (Figure S2).

Relative to 1-D SEB AWS, the more complex physics in HIRHAM5 result in multiple possible causes of melt rate underestimation. Importantly, RCM simulations rely on calculated, rather than measured, radiative components. For instance, the MODIS-derived July mean albedo employed by HIRHAM5 at, e.g., QAS_L is 0.44, which is a factor of 2 higher than the observed value of 0.21 [*Van As et al*., 2013]. Also, the parameterized z_0 for ice is a factor of 5 lower than the value adopted in the 1-D SEB_{AWS} model, which could result in estimates of smaller turbulent heat fluxes. Finally, the digital elevation model used by HIRHAM5 overestimates the elevation at, e.g., QAS_L by ~120 m, which also contributes to underestimated melt rates due to near-surface temperature underestimation in HIRHAM5. Substantial uncertainty is associated with rain energy fluxes during the exceptional melt episodes in both the RCM and 1-D SEB_{AWS} simulations. For example, observations from Qaqortoq, ~60 km southwest of QAS_L, reported ~20 mm rain during the 8–11 July episode E1 and ~50 mm rain during the 27–28 July episode E2 (www.dmi.dk). The total amount of rainfall simulated by HIRHAM5 at QAS_L was 192 and 186 mm during both respective episodes. With such large rainfall rates, it is possible that rain energy flux contributed to more melt than either model calculates because both models assume rain temperature to be equal to the near-surface air temperature, which, in the presence of temperature inversions, is likely less than the actual temperature of the rain. Weather balloon measurement from the integrated global radiosonde archive [*Durre et al*., 2006] for Narsarsuaq (~80 km to the east) shows a temperature inversion (up to 5°C) during both melt episodes.

The melt episodes observed at AWSs and illustrated in Figure 2 in all of west and south Greenland in 2012 are consistent with the observations of *Tedesco et al*. [2013], who show that the 2012 ice sheet-wide melt, air temperature, runoff, and albedo were unprecedented in the past decades and resulted from anomalous persistent high air pressure over Greenland, which provided stable weather with relatively low cloud cover and high solar radiation. This systematic and persistent change in Arctic atmospheric circulation, due to regional atmospheric blocking, was dominant during the 2007–2012 period, and resulted in the advection of warm southern air masses toward Greenland [*Overland et al*., 2012; *Hanna et al*., 2012, 2014; *Fettweis et al*., 2013; *Häkkinen et al*., 2014; *Rajewicz and Marshall*, 2014]. The contrasting melt sensitivity of nonradiative energy fluxes between western and eastern PROMICE stations indicates less frequent warm and moist air advections in east Greenland due to more stable weather, possibly supplemented by a stronger katabatic wind influence that mitigates the potential impact of nonradiative energy fluxes [*Noël et al*., 2014]. More broadly, data from the two episodes presented here demonstrate that exceptional melt can occur during periods characterized by cloudy skies and transient atmospheric flow, with melt being dominated by nonradiative, rather than radiative fluxes in the ablation area.

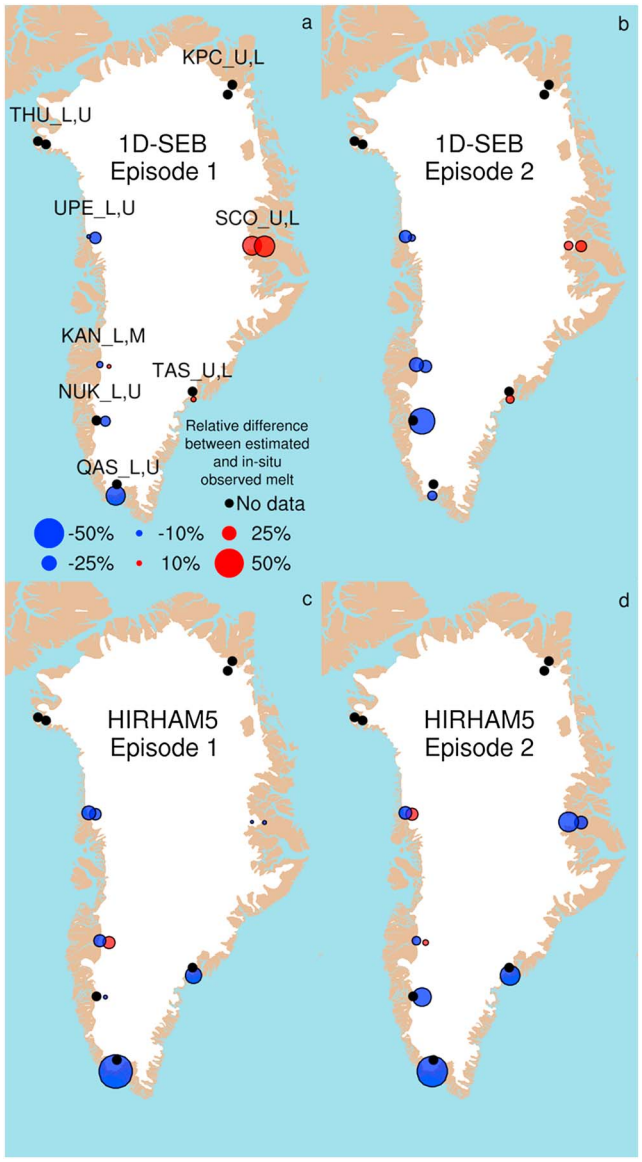

Figure 3. Relative difference (%) between the estimated ablation for 1-D SEB_{AWS} and the HIRHAM5 RCM and insitu ablation observations for the exceptional melt episodes E1 and E2. Negative and positive numbers overestimate and underestimate melt, respectively. Graphics illustrates the values in Table S2.

3.3. Implications for Melt Projections

Figure 3 illustrates the relative mismatch between in situ ablation observations and estimated ablation from 1-D SEB_{AWS} and HIRHAM5 for all PROMICE locations with available data.

The mismatch between 1-D SEB_{AWS} calculations and in situ ablation observations at southern and western ice sheet locations (QAS_L, NUK_U, KAN_L, UPE_L, and UPE_U) implies an average underestimation of 18% for both episodes (Table S2). This excludes the first melt episode at KAN_M, because it was dominated by radiative energy fluxes (Table S1). The highest underestimation of ablation is 43% at NUK_U, while the lowest is 7% at UPE_L (Figures 3a, 3b, and Table S2). However, the largest absolute melt underestimation of 0.3 m ice eq. or 33% is found at QAS_L. In contrast, for eastern Greenland ice sheet sites the 1-D SEB_{AWS} overestimates ablation, which is dominated by radiative fluxes. The largest overestimation is found at the eastern ice sheet SCO sites during E1; however, the absolute melt contribution is relatively small, which results in relatively large differences between modeled and observed ablation (Figures 3a, 3b, and Table S2). The aerodynamic roughness length z_0 seems to be too large at the east coast, resulting in an overestimation of the nonradiative fluxes. Choosing a single z_0 for all of Greenland is problematic and would explain the overestimation of melt as the east coast (SCO_L,U and TAS_L), which did not experience the two exceptional melt events (Figure 2c). During the two melt events at the west coast (Figure 2b), the daily mismatch between modeled and in situ observed melt cannot be explained by a larger constant z_0. To minimize the mismatch between the modeled and in situ observed daily melt, would require a significantly larger z_0, which should then be reset to its original value when the melt episode is over.

In general, HIRHAM5 underestimates melt in the ablation area, although a direct comparison with point data is difficult because at 5.5 km resolution HIRHAM5 underestimates total melt during the two melt episodes by up to 56% in the south, while the average for both episodes is 17% (Table S2). For west Greenland PROMICE sites, this may be a combination of underestimated E_{NonRad}, underestimated net downward radiative fluxes (due to too high albedo) [*Langen et al.*, 2015] and unresolved topographical effects in the ablation area. For the east Greenland sites, the underestimated melt is mostly due to the latter two since E_{NonRad} had a minor influence here (Figure 2). The HIRHAM5 melt underestimation is typical for RCMs [e.g., *Fettweis et al.*, 2011; *van As et al.*, 2014; *Noël et al.*, 2015]. E_{NonRad} is thus likely responsible for an even greater proportion of melt than RCMs capture during exceptional episodes.

RCM simulations suggest that climate change will likely result in an increase in wind speeds around the Greenland ice sheet periphery [*Gorter et al*., 2013]. Further, cyclonic activity around Greenland is projected to increase future precipitation rates [*Schuenemann and Cassano*, 2010; *Vavrus*, 2013]. Combined with increases in air temperature over the ice sheet ablation area, the melt energy from turbulent and rain energy fluxes should increase. Our study demonstrates that even at an ice sheet location, such as QAS_L, with very low-bare ice albedo (~0.2), where absorbed solar radiation is relatively large in comparison to the rest of the ice sheet, the studied melt episodes are mostly driven by nonradiative energy fluxes. Melt driven by atmospheric heat and moisture advection therefore made up a significant fraction of annual ablation (12–15%, Table 1). Critically, nonradiative energy fluxes from the 1-D SEB AWS dominated south and west Greenland and are on average underestimated by 14% and 22% for episodes E1 and E2, respectively (Table S2). Furthermore, HIRHAM5 underestimates this percentage at some locations even more, as it is known to underestimate mass loss from high-melt areas of the ice sheet in comparison to 1-D SEB_{AWS}s [*Van As et al*., 2014; *Langen et al*., 2015]. However, the average melt underestimation in HIRHAM5 ended up being smaller than in the 1-D SEB_{AWS} (Table S2).

There has been a range of estimates for the surface mass balance of Greenland using RCMs [e.g., *Fettweis et al*., 2011; *Vernon et al*., 2013; *Rae et al*., 2012; *Enderlin et al*., 2014; *van As et al*., 2014; *Langen et al*., 2015]. Results from *Noël et al*. [2015] and *Fettweis et al*. [2011] indicate that at least two other RCMs commonly used in Greenland ice sheet analyses may also underestimate the contribution from the turbulent fluxes to melt of glacier surfaces during extreme episodes.

According to HIRHAM5, 1153 Gt of snow and ice melted on the Greenland ice sheet in 2012. The two melt episodes at the western PROMICE sites resulted in ~14% (161 Gt) of the annual ice sheet melt (Table 1). On top of this, we estimate the systematic 1-D SEB_{AWS} underestimation of 18% to reach roughly 15 Gt of melt underestimation per melt episode. Since melt episodes are anticipated to become more frequent in the future [*McGrath et al*., 2013], there is a strong impetus to ensure that nonradiative energy fluxes are accurately simulated in climate projections.

4. Conclusions

We find that year 2012 Greenland ice sheet melt was marked not only by widespread interior surface melting [*Nghiem et al*., 2012] but also by an increased nonradiative (sensible, latent, and rain) energy flux contributing to melt in the ablation area of the southern and western ice sheet. Latent and sensible energy advection governed two exceptional melt episodes in July 2012 [*Neff et al*., 2014]. The two episodes which lasted just ~6% of the ablation period in June–August were responsible for ~14% of the annual 2012 ablation average for all PROMICE measurement sites (Table 1). At all PROMICE sites during the two exceptional melt episodes the combined sensible, latent, rain, and subsurface energy fluxes (i.e., nonradiative energy fluxes) comprised 60% of the melt energy on average (Figure 1 and Table S1).

A HIRHAM5 regional climate model simulation corroborates these findings and suggests that these two exceptional melt episodes were dominated by nonradiative fluxes over approximately one third of the Greenland ice sheet ablation area (Figure 2a). However, in comparison with independent in situ ablation measurements, both the weather station-driven one-dimensional surface energy budget (1-D SEB_{AWS}) calculation and the HIRHAM5 RCM underestimate melt by 18% and 16%, respectively, through an underestimation of nonradiative surface heating during these exceptional episodes for the western part of the ice sheet (Figure 3 and Table S2). Given projected increases in wind speed and cyclonic activity, climate change increases the frequency of strong melt episodes dominated by nonradiative energy fluxes [*Schuenemann and Cassano*, 2010; *Gorter et al*., 2013; *Vavrus*, 2013]. This provides a strong impetus to consider the accuracy with which such episodes are represented within conventional model frameworks [*Hanna et al*., 2014]. Given that exceptional melt episodes appear to be responsible for a significant fraction of total melt, a failure to accurately simulate them may result in larger uncertainties in projected Greenland sea level contribution.

Acknowledgments

We would like to thank two anonymous reviewers and Editor, Julienne Stroeve, for their valuable comments, which improved the study significantly. PROMICE is funded by the Danish Ministry of Climate, Energy and Building under Danish Cooperation for Environment in the Arctic (DANCEA) and is operated by the Geological Survey of Denmark and Greenland (GEUS) in collaboration with the National Space Institute (DTU Space) and Asiaq (Greenland Survey). KAN weather station data are chiefly funded by the Greenland Analogue Project (GAP). PROMICE data are freely accessible at http://promice.org. HIRHAM5 simulations were carried out under the Nordforsk project SVALI and the Danish funded Greenland Climate Research Centre project. The Danish Council for Independent research (DFF) project 4002-00234 is also acknowledged for partial support of this study.

References

Ahlstrøm, A. P., et al. (2008), A new programme for monitoring the mass loss of the Greenland ice sheet, *Geol. Surv. Den. Greenl. Bull.*, *15*, 61–64.

Andersen, M. L., et al. (2015), Basin-scale partitioning of Greenland ice sheet mass balance components (2007–2011), *Earth Planet. Sci. Lett.*, *409*, 89–95, doi:10.1016/j.epsl.2014.10.015.

Andreas, J. L. (2002), Parameterizing scalar transfer over snow and ice: A review, *J. Hydrometeorol.*, *3*, 417–432.

Bennartz, R., M. D. Shupe, D. D. Turner, V. P. Walden, K. Steffen, C. J. Cox, M. S. Kulie, N. B. Miller, and C. Pettersen (2013), July 2012 Greenland melt extent enhanced by low-level liquid clouds, *Nature*, *496*, 83–86, doi:10.1038/nature12002.

Bonne, J. L., et al. (2015), The summer 2012 Greenland heat wave: In situ and remote sensing observations of water vapor isotopic composition during an atmospheric river event, *J. Geophys. Res. Atmos.*, *120*, 2970–2989, doi:10.1002/2014JD022602.

Box, J. E., X. Fettweis, J. C. Stroeve, M. Tedesco, D. K. Hall, and K. Steffen (2012), Greenland ice sheet albedo feedback: Thermodynamics and atmospheric drivers, *Cryosphere*, *6*, 821–839.

Brock, B. W., I. C. Willis, and M. J. Shaw (2006), Measurement and parameterization of aerodynamic roughness length variations at Haut Glacier d'Arolla, Switzerland, *J. Glaciol.*, *52*, 281–297.

Collins, M., et al. (2013), Long-term climate change: Projections, commitments and irreversibility, in *Climate Change 2013: The Physical Science Basis. Contribution of Working Group I to the Fifth Assessment Report of the Intergovernmental Panel on Climate Change*, edited by T. F. Stocker et al., 1535 pp., Cambridge Univ. Press, Cambridge, U. K., doi:10.1017/CBO9781107415324.

Durre, I., R. S. Vose, and D. B. Wuertz (2006), Overview of the integrated global radiosonde archive, *J. Clim.*, *19*, 53–68, doi:10.1175/JCLI3594.1.

Dutton, A., A. E. Carlson, A. J. Long, G. A. Milne, P. U. Clark, R. DeConto, B. P. Horton, S. Rahmstorf, and M. E. Raymo (2015), Sea-level rise due to polar ice-sheet mass loss during past warm periods, *Science*, *349*(6244), doi:10.1126/science.aaa4019.

Elvidge, A. D., I. A. Renfrew, A. I. Weiss, I. M. Brooks, T. A. Lachlan-Cope, and J. C. King (2015), Observations of surface momentum exchange over the marginal-ice-zone and recommendations for its parameterization, *Atmos. Chem. Phys. Discuss.*, *15*, 26,609–26,660, doi:10.5194/acpd-15-26609-2015.

Enderlin, E. M., I. M. Howat, S. Jeong, M. J. Noh, J. H. van Angelen, and M. R. van den Broeke (2014), An improved mass budget for the Greenland ice sheet, *Geophys. Res. Lett.*, *41*, 866–872, doi:10.1002/2013GL059010.

Fausto, R. S., D. van As, A. P. Ahlstrøm, S. B. Andersen, M. L. Andersen, M. Citterio, K. Edelvang, H. Machguth, S. Nielsen, and A. Weidick (2012a), Ablation observations for 2008–2011 from the Programme for Monitoring of the Greenland Ice Sheet (PROMICE), *Geol. Surv. Den. Greenl. Bull.*, *26*, 25–28.

Fausto, R. S., D. van As, A. P. Ahlstrøm, and M. Citterio (2012b), Assessing the accuracy of Greenland ice sheet ice ablation measurements by pressure transducers, *J. Glaciol.*, *58*(212), 1144–1150.

Fettweis, X., M. Tedesco, M. R. van den Broeke, and J. Ettema (2011), Melting trends over the Greenland ice sheet (1958–2009) from spaceborne microwave data and regional climate models, *Cryosphere*, *5*, 359–375, doi:10.5194/tc-5-359-2011.

Fettweis, X., E. Hanna, C. Lang, A. Belleflamme, M. Erpicum, and H. Gallée (2013), Important role of the mid-tropospheric atmospheric circulation in the recent surface melt increase over the Greenland ice sheet, *Cryosphere*, *7*, 241–248.

Gorter, W., J. H. van Angelen, J. T. M. Lenaerts, and M. R. van den Broeke (2013), Present and future near-surface wind climate of Greenland from high resolution regional climate modelling, *Clim. Dyn.*, doi:10.1007/s00382-013-1861-2.

Häkkinen, S., D. K. Hall, C. A. Shuman, D. L. Worthen, and N. E. DiGirolamo (2014), Greenland ice sheet melt from MODIS and associated atmospheric variability, *Geophys. Res. Lett.*, *41*, 1600–1607, doi:10.1002/2013GL059185.

Hanna, E., J. M. Jones, J. Cappelen, S. H. Mernild, L. Wood, K. Steffen, and P. Huybrechts (2012), The influence of North Atlantic atmospheric and oceanic forcing effects on 1900–2010 Greenland summer climate and ice melt/runoff, *Int. J. Climatol.*, doi:10.1002/joc.3475.

Hanna, E., X. Fettweis, S. H. Mernild, J. Cappelen, M. H. Ribergaard, C. A. Shuman, K. Steffen, L. Wood, and T. L. Mote (2014), Atmospheric and oceanic climate forcing of the exceptional Greenland ice sheet surface melt in summer 2012, *Int. J. Climatol.*, doi:10.1002/joc.3743.

Hartmann, D. L., et al. (2013), Observations: Atmosphere and surface, in *Climate Change 2013: The Physical Science Basis. Contribution of Working Group I to the Fifth Assessment Report of the Intergovernmental Panel on Climate Change*, edited by T. F. Stocker et al., 1535 pp., Cambridge Univ. Press, Cambridge, U. K., doi:10.1017/CBO9781107415324.

Keegan, K. M., M. R. Albert, J. R. McConnell, and I. Baker (2014), Climate change and forest fires synergistically drive widespread melt events of the Greenland ice sheet, *Proc. Natl. Acad. Sci. U.S.A.*, *111*, 7964–7967.

Khan, S. A., A. Aschwanden, A. A. Bjørk, J. Wahr, K. K. Kjeldsen, and K. H. Kjær (2015), Greenland ice sheet mass balance: A review, *Rep. Prog. Phys.*, *78*(4), 046801.

Langen, P. L., et al. (2015), Quantifying energy and mass fluxes controlling Godthåbsfjord freshwater input in a 5 km simulation (1991–2012), *J. Clim.*, doi:10.1175/JCLI-D-14-00271.1.

Lenaerts, J. T. M., D. LeBars, L. van Kampenhout, M. Vizcaino, E. M. Enderlin, and M. R. van den Broeke (2015), Representing Greenland ice sheet freshwater fluxes in climate models, *Geophys. Res. Lett.*, *42*, 6373–6381, doi:10.1002/2015GL064738.

Lucas-Picher, P., M. Wulff-Nielsen, J. H. Christensen, G. Aðalgeirsdóttir, R. Mottram, and S. Simonsen (2012), Very high resolution in regional climate model simulations for Greenland—Identifying added value, *J. Geophys. Res.*, *117*, D02108, doi:10.1029/2011JD016267.

Lüpkes, C., V. M. Gryanik, J. Hartmann, and E. L. Andreas (2012), A parametrization, based on sea ice morphology, of the neutral atmospheric drag coefficients for weather prediction and climate models, *J. Geophys. Res.*, *117*, D13112, doi:10.1029/2012JD017630.

Machguth, H., M. MacFerrin, D. van As, J. E. Box, C. Charalampidis, W. Colgan, R. S. Fausto, H. A. J. Meijer, E. Mosley-Thompson, and R. S. W. van de Wal (2016), Greenland meltwater storage in firn limited by near-surface ice formation, *Nat. Clim. Change*, doi:10.1038/nclimate2899.

McGrath, D., W. Colgan, N. Bayou, A. Muto, and K. Steffen (2013), Recent warming at Summit, Greenland: Global context and implications, *Geophys. Res. Lett.*, *40*, 2091–2096, doi:10.1002/grl.50456.

Neff, W., G. P. Compo, F. M. Ralph, and M. D. Shupe (2014), Continental heat anomalies and the extreme melting of the Greenland ice surface in 2012 and 1889, *J. Geophys. Res. Atmos.*, *119*, 6520–6536, doi:10.1002/2014JD021470.

Nghiem, S. V., D. K. Hall, T. L. Mote, M. Tedesco, M. R. Albert, K. Keegan, C. A. Shuman, N. E. DiGirolamo, and G. Neumann (2012), The extreme melt across the Greenland ice sheet in 2012, *Geophys. Res. Lett.*, *39*, L20502, doi:10.1029/2012GL053611.

Noël, B., X. Fettweis, W. J. van de Berg, M. R. van den Broeke, and M. Erpicum (2014), Sensitivity of Greenland ice sheet surface mass balance to perturbations in sea surface temperature and sea ice cover: A study with the regional climate model MAR, *Cryosphere*, *8*, 1871–1883, doi:10.5194/tc-8-1871-2014.

Noël, B., W. J. van de Berg, E. van Meijgaard, P. Kuipers Munneke, R. S. W. van de Wal, and M. R. van den Broeke (2015), Evaluation of the updated regional climate model RACMO2.3: Summer snowfall impact on the Greenland Ice Sheet, *Cryosphere*, *9*, 1831–1844, doi:10.5194/tc-9-1831-2015.

Overland, J. E., J. A. Francis, E. Hanna, and M. Wang (2012), The recent shift in early summer Arctic atmospheric circulation, *Geophys. Res. Lett.*, *39*, L19804, doi:10.1029/2012GL053268.

Rae, J. G. L., et al. (2012), Greenland ice sheet surface mass balance: Evaluating simulations and making projections with regional climate models, *The Cryosphere*, *6*, 1275–1294, doi:10.5194/tc-6-1275-2012.

Rajewicz, J., and S. J. Marshall (2014), Variability and trends in anticyclonic circulation over the Greenland ice sheet, 1948–2013, *Geophys. Res. Lett.*, *41*, 2842–2850, doi:10.1002/2014GL059255.

Roeckner, E., et al. (2003), The atmospheric general circulation model ECHAM5. Part I: Model description, *Rep. 349*, Max-Planck-Inst. für Meteorol., Hamburg.

Schuenemann, K. C., and J. J. Cassano (2010), Changes in synoptic weather patterns and Greenland precipitation in the 20th and 21st centuries: 2. Analysis of 21st century atmospheric changes using self-organizing maps, *J. Geophys. Res.*, *115*, D05108, doi:10.1029/2009JD011706.

Smeets, C. J. P. P., and M. R. van den Broeke (2008), Temporal and spatial variation of momentum roughness length in the ablation zone of the Greenland ice sheet, *Boundary Layer Meteorol.*, *128*, 315–338.

Tedesco, M., X. Fettweis, T. Mote, J. Wahr, P. Alexander, J. E. Box, and B. Wouters (2013), Evidence and analysis of 2012 Greenland records from spaceborne observations, a regional climate model and reanalysis data, *Cryosphere*, *7*, 615–630.

Tjernström, M., et al. (2015), Warm-air advection, air mass transformation and fog causes rapid ice melt, *Geophys. Res. Lett.*, *42*, 5594–5602, doi:10.1002/2015GL064373.

Van As, D., A. L. Hubbard, B. Hasholt, A. B. Mikkelsen, M. R. van den Broeke, and R. S. Fausto (2012), Large surface meltwater discharge from the Kangerlussuaq sector of the Greenland ice sheet during the record-warm year 2010 explained by detailed energy balance observations, *Cryosphere*, *6*, 199–209.

Van As, D., et al. (2013), Darkening of the Greenland ice sheet due to the melt albedo feedback observed at PROMICE weather stations, *Geol. Surv. Den. Greenl. Bull.*, *28*, 69–72.

Van As, D., et al. (2014), Increasing meltwater discharge from the Nuuk region of the Greenland ice sheet and implications for mass balance (1960–2012), *J. Glaciol.*, *60*(220), 314–322, doi:10.3189/2014JoG13J065.

Van den Broeke, M., C. J. P. P. Smeets, J. Ettema, C. van der Veen, R. S. W. van de Wal, and J. Oerlemans (2008), Partitioning of melt energy and meltwater fluxes in the ablation zone of the west Greenland ice sheet, *Cryosphere*, *2*, 179–189, doi:10.5194/tc-2-179-2008.

Van den Broeke, M. R., D. van As, C. H. Reijmer, and R. S. W. van de Wal (2004), Assessing and improving the quality of unattended radiation observations in Antarctica, *J. Atmos. Oceanic Technol.*, *21*(9), 1417–1431.

Van den Broeke, M. R., C. J. P. P. Smeets, and R. S. W. van de Wal (2011), The seasonal cycle and interannual variability of surface energy balance and melt in the ablation area of the west Greenland ice sheet, *Cryosphere*, *5*(2), 377–390, doi:10.5194/tc-5-377-2011.

Vavrus, S. J. (2013), Extreme Arctic cyclones in CMIP5 historical simulations, *Geophys. Res. Lett.*, *40*, 6208–6212, doi:10.1002/2013GL058161.

Vernon, C. L., J. L. Bamber, J. E. Box, M. R. van den Broeke, X. Fettweis, E. Hanna, and P. Huybrechts (2013), Surface mass balance model intercomparison for the Greenland ice sheet, *The Cryosphere*, *7*, 599–614, doi:10.5194/tc-7-599-2013.